Available online at www.sciencedirect.com
SCIENCE DIRECT®
Journal of Membrane Science 277 (2006) 18–27
journal of MEMBRANE SCIENCE
www.elsevier.com/locate/memsci

Electrolyte retention of supported bi-layered nanofiltration membranes

W.B. Samuel de Lint [a,1], Tijana Zivkovic [a], Nieck E. Benes [b], Henny J.M. Bouwmeester [a], Dave H.A. Blank [a,*]

[a] *Laboratory of Inorganic Materials Science, Department of Chemical Technology & MESA+ Institute for Nanotechnology, University of Twente, P.O. Box 217, 7500 AE Enschede, The Netherlands*
[b] *Process Development Group, Department of Chemical Engineering and Chemistry, Technical Eindhoven University of Technology, P.O. Box 513, 5600 MB Eindhoven, The Netherlands*

Received 19 April 2005; received in revised form 30 August 2005; accepted 4 October 2005
Available online 14 November 2005

Abstract

The electrolyte separation behaviour of a supported bi-layered ceramic membrane is investigated experimentally and the measured ion retentions are compared with the predictions of a site-binding transport model with no adjustable parameters. Due to the difference in iso-electric point between its two separating layers, the bi-layered system is expected to perform better over a large pH range compared with a membrane with only one type of selective layer. The separating layers in the membrane are a microporous silica and a mesoporous γ-alumina (pore sizes of 0.8 and 2 nm, respectively) and their retention is studied for a binary electrolyte solution of NaCl at 1 mol/m^3 for pH values between 4 and 10.

Because of its smaller pores and high charge, the silica layer mainly determines the membrane retention at neutral and alkaline pH, while the γ-alumina layer has a significant impact on the NaCl retention at $4 < pH < 5$. The model predictions are in good agreement with the experimental data for Na^+ at $4 < pH < 9$ and for Cl^- at the whole pH range. For a pH of 4, the predicted chloride retention is lower than the sodium retention while the experimental data show the opposite effect.

Keywords: Bi-layered; Nanofiltration; Modelling; Mass transfer; Ion adsorption

1. Introduction

The last decade considerable progress has been made in understanding and predicting the ion separation of nanofiltration (NF) membranes. For the separation of salts from aqueous solutions using inorganic NF membranes consensus is that separation arises mainly from electrostatic interactions between ions and the charged membrane. A NF membrane performs ion separation best at pH values far from its iso-electric point (IEP), as this corresponds to a high membrane potential. Apart from the pH, the membrane potential and charge is also a strong function of the type of ions present in the electrolyte solution and their concentration [1–9].

For titania, a now commonly used membrane material, the IEP is around 6 [6,7]. As the pH of most aqueous electrolyte solutions (without any addition of acid or base) is also close to 6, titania membranes will perform very poorly in a practical application. In general, inorganic NF membranes suffer from this problem as their IEPs are close to pH 7 (cf. titania, but also zirconia (IEP ≈ 6) and γ-alumina (IEP ≈ 8)). Additionally, in industrial applications one would like to use a membrane over a large pH range (e.g., to selectively remove differently charged species). In this case the membrane's IEP is often included in the operating pH range and consequently the membrane separation performance will be poor there.

A solution for both of these problems is to use a membrane consisting of a mixture of two materials with a different IEP. However, Elmarraki et al. [10] showed that this option may not be a viable alternative as one of the two materials in a mixed system can dominate the charging properties of the membrane layer (see Fig. 6 in their work). A more promising option could be to create a stack of layers of materials with a different IEP [11,12]. In addition to the expected improved separation performance, This may also be a fast and effective way to reduce the exposure of any intermediate layers to harsh pH conditions (due to retention, the top layer can reduce the concentration of strong acid or base

* Corresponding author. Tel.: +31 53 489 3121/2860; fax: +31 53 4894683.
E-mail address: d.h.a.blank@utwente.nl (D.H.A. Blank).
[1] Unilever Corporate Research, Colworth House, Sharnbrook, Bedford MK44 1LQ, UK.

0376-7388/$ – see front matter © 2005 Elsevier B.V. All rights reserved.
doi:10.1016/j.memsci.2005.10.004

within the next layers) or, alternatively to prevent fouling of the membrane [13].

It must be noted here that the separation performance of any membrane with one or more positive and negative layers can be significantly reduced by strongly adsorbing electrolytes that may nullify or reverse the charge on some of these layers. Such effects are well known for monopolar membranes but Elmarraki et al. [14] have also shown this for bilayered membranes.

The advantages of a two-layer NF membrane system were the incentive to conduct an investigation into the separation characteristics of these membranes. Adopting the extended Nernst–Planck equations Tsuru et al. [15] presented a thorough theoretical analysis of the retention behaviour of bilayered (bipolar) reverse osmosis membranes, showing the effects of flux, concentration and potential on their separation performance. They did however not discuss the effect of membrane charge on retention or compared their predictions to experimental data.

As the membrane charge is strongly dependent on the pH, in this work the electrolyte retention of a bilayered membrane is studied as a function of pH. The membrane used in this study consists of a silica and a γ-alumina separating layer and its retention behaviour is studied for the monovalent electrolyte NaCl. The experimental data is compared with predictions of the model presented by De Lint and Benes [8], which is extended to incorporate the charging effects of both separating layers.

2. Theory

In the model applied in this work [8], the charge on nanofiltration membranes is determined by adsorption of protons and electrolyte ions on a fixed number of sites, $c_{\mathrm{tot}}^{//}$. Adsorption is assumed to occur on a single type of surface site, M–$OH^{-1/2}$ [16], with M representing either alumina or silica. The exact surface structure of silica is not known but it is thought that its charging behaviour is fully dominated by Si–O^- groups [17]. Here, for simplicity however we assume that alumina and silica have the same active surface site for adsorption, being M–$OH^{-1/2}$. On this surface site competitive adsorption of protons, cations (here Na^+) and anions (here Cl^-) takes place. In this work adsorption is described by the well-known $1-pK$ site-binding model:

$$\begin{aligned} &\mathrm{M-OH^{-1/2}} + \mathrm{H^+(s)} \overset{K_1^+}{\rightleftharpoons} \mathrm{M-OH_2{}^{+1/2}} \\ &\mathrm{M-OH^{-1/2}} + \mathrm{Na^+(s)} \overset{K_{\mathrm{Na}}}{\rightleftharpoons} \mathrm{M-OH^{-1/2}Na^+} \\ &\mathrm{M-OH_2{}^{+1/2}} + \mathrm{Cl^-(s)} \overset{K_{\mathrm{Cl}}}{\rightleftharpoons} \mathrm{M-OH_2{}^{+1/2}Cl^-} \end{aligned} \quad (1)$$

A label (s) in Eq. (1) is used to designate virtual non-adsorbed ions (e.g., H^+) with the same potential as their surface complexes (e.g., M–$OH_2{}^{+1/2}$). The corresponding equilibrium constants are:

$$K^+ = \frac{c^{\mathrm{ref}} c_{\mathrm{M-OH_2{}^{+1/2}}}}{c^{\mathrm{s}}_{\mathrm{H^+}} c_{\mathrm{M-OH^{-1/2}}}}, \quad K_{\mathrm{Na}} = \frac{c^{\mathrm{ref}} c_{\mathrm{M-OH^{-1/2}Na^+}}}{c^{\mathrm{s}}_{\mathrm{Na^+}} c_{\mathrm{M-OH^{-1/2}}}},$$

$$K_{\mathrm{Cl}} = \frac{c^{\mathrm{ref}} c_{\mathrm{M-OH_2{}^{+1/2}Cl^-}}}{c^{\mathrm{s}}_{\mathrm{Cl^-}} c_{\mathrm{M-OH_2{}^{+1/2}}}}, \quad (2)$$

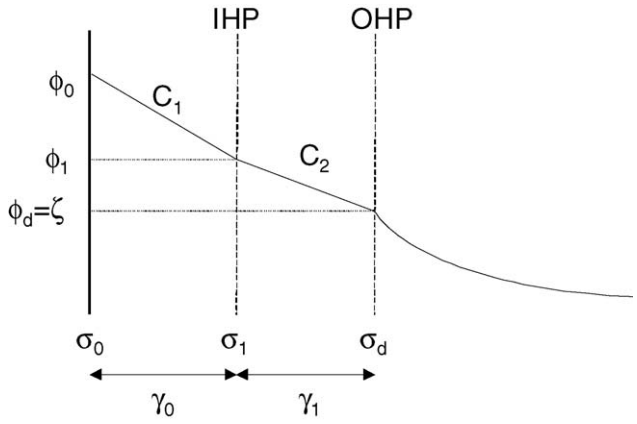

Fig. 1. Schematic description of triple-layer model consisting of an inner and outer Helmholtz plane (IHP and OHP, respectively), comprising the so-called Stern layer, and a diffuse double layer (not drawn to scale).

with c^{ref} the thermodynamic reference concentration of 10^3 mol/m^3 (1 mol/dm^3). In the $1-pK$ model the proton adsorption constant is equal to the point of zero charge, $pH_{PZC} = pK^+$ The Boltzmann relation relates the concentration of virtual species to that in the bulk of the electrolyte.

$$c_i^{\mathrm{s}} = \gamma_i c_i^b \exp\left(\frac{-z_i F}{RT}\phi_{\mathrm{s}}\right). \quad (3)$$

In Eq. (3), γ_i, is the bulk activity coefficient of species i; b denotes the bulk ($\phi_{\mathrm{b}} \equiv 0$), z_i, the charge number; F, the constant of Faraday; R, the ideal gas constant; T, the temperature, and ϕ_{s}, the potential of the virtual species c_i^{s}. In this work we assume a thermodynamically ideal solution that is $\gamma_i \equiv 1$.

To describe the variation of the potential ϕ and charge σ away from the membrane pore surface a triple-layer model (see Fig. 1) is adopted [16], consisting of the surface or 0-plane, the 1-plane or inner Helmholtz plane (IHP), the 2-plane or outer Helmholtz plane (OHP) and a layer with diffuse charge (σ_{d}). Adsorbed protons are located at the 0-plane while electrolyte adsorption occurs on the 1-plane. The electrostatic expressions for the charge σ_{p} at the planes for the triple-layer model are:

$$\sigma_0 = C_1(\phi_0 - \phi_1), \quad (4)$$

$$\sigma_1 = C_2(\phi_1 - \phi_2) - C_1(\phi_0 - \phi_1), \quad (5)$$

$$\sigma_2 = 0. \quad (6)$$

In this work, the location of the shear or zeta potential plane, ζ, is assumed to be located near the OHP, but is a function of the electrolyte concentration (see [16]). Due to double layer overlap, the radial potential in the diffuse part of the double layer can be assumed constant. This assumption of zero radial potential gradient is referred to as the uniform potential approach and results in a diffuse double layer charge σ_{d} given by

$$\sigma_{\mathrm{d}} = \frac{a}{2} cF \sum_{i=1}^{n} z_i x_i, \quad (7)$$

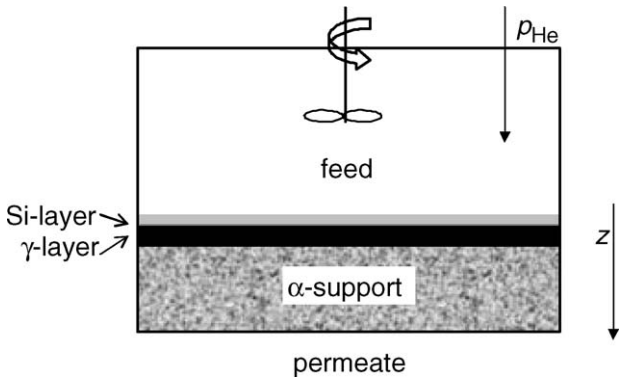

Fig. 2. Model of dead-end membrane permeation set-up with bilayered membrane.

where a is the membrane pore radius (assuming cylindrical pores), x_i is the molar fraction of species i, and c is the total concentration.

A crucial point in properly linking the charging properties to the transport behaviour in our NF model is the effect of charge regulation. This concept, describing the variation of double layer charge and potential as charged surfaces approach each other (e.g., [18,19]), allows the use of (zeta) potential and (surface) charge data of particles in dilute electrolyte solutions for the prediction of the charging properties in NF membrane pores with double layer overlap [16].

For the description of transport in this work the Maxwell–Stefan relations in one-dimension (the direction of flow, z, see Fig. 2) are used:

$$-\frac{\mathrm{d}x_i}{\mathrm{d}z}-\frac{\bar{V}_i}{RT}x_i\frac{\mathrm{d}p}{\mathrm{d}z}-\frac{F}{RT}x_i z_i\frac{\mathrm{d}\phi}{\mathrm{d}z}-H_i^c\frac{x_i}{Đ_{i\mathrm{M}}^{\mathrm{eff}}}v = \sum_{j=1}^{n}\frac{x_j N_i - x_i N_j}{cĐ_{ij}^{\mathrm{eff}}}+\frac{N_i}{cĐ_{i\mathrm{M}}^{\mathrm{eff}}}, \tag{8}$$

with $\bar{V}_i$ the molar volumes, z_i the charge number, H_i^c a correction factor for convective transport, v the convective velocity, N_i are the species' fluxes, and $Đ_{ij}^{\mathrm{eff}}$ are the effective Maxwell–Stefan diffusion coefficients. In the model the solvent and solute activity coefficients are assumed unity and radial pore potential gradients are neglected [5,8]. For the pore sizes used in this study (<2 nm) this uniform potential approach can be confidently used (see Fig. 9b in [5]). Other major assumptions in the model include: isothermal dead-end filtration system, cylindrical membrane pores, steady state ($\mathrm{d}N_i/\mathrm{d}z = 0$), external mass transport represented by a stagnant film of 10 μm thickness. For a detailed description and derivation of Eq. (8), the reader is referred to [8].

For our bi-layered membrane there are three interfaces (see Fig. 2): the feed/silica interface, the silica/γ-alumina interface and the γ-alumina/support interface. At all these interfaces we assume local thermodynamic equilibrium.

$$x_i^{(+)} = h_i x_i^{(-)} \exp\left[\frac{-z_i F}{RT}\phi^{(+)}-\phi^{(-)}\right]\exp\left[\frac{-\bar{V}_i}{RT}(p^{(+)}-p^{(-)})\right], \tag{9}$$

where the superscripts (+) and (−) denote locations just inside and outside the interface, respectively, and the term h_i, accounts for steric hindrance effects.

Some additional relations are needed to complete our model description but here only the key equations are given here. For amore detailed description of the model the reader is referred to [8].

Electroneutrality must hold everywhere in the system.

$$\sum_{i=1}^{n} z_i x_i = 0. \tag{10}$$

The boundary conditions are considered at the feed and the permeate. The feed concentrations, pressure and potential are fixed. In the permeate 'e', the concentrations are related to the fluxes,

$$\frac{N_i}{N_j} = \frac{x_i^{\mathrm{e}}}{x_j^{\mathrm{e}}}. \tag{11}$$

The pressure at the permeate 'e' side is atmospheric. The boundary condition for the permeate potential is provided by the electroneutrality equation, Eq. (10). It can be shown (see [8]) using Eqs. (10) and (11) that the zero-current relation is implicitly accounted for in this model.

The model equations are solved for the molar fractions x_i, the uniform pore potential ϕ, and the pressure p in both separating layers of the membrane as well as in the support. Only in both separating layers the charge regulation expressions are used to calculate the radial potentials (ϕ_0, ϕ_1) and charge (σ_0, σ_1) in the double layer (when employing the triple-layer model). The molar fluxes N_i the pressure in the support p^{s}, and the permeate potential ϕ^{e} are the other variables in the model. The model is implemented in the mathematical software programme Maple (Waterloo Maple, Ont., Canada) and is freely available at: http://www.ims.tnw.utwente.nl/publication/downloads.

2.1. Effect of two separating layers on ion retention

The main idea of applying a bi-layered NF membrane with separating layers featuring a different iso-electric point (IEP) is that such a system will perform better over a large pH range compared to a membrane with only one IEP. To show this characteristic, in Fig. 3 the transport model is applied to calculate the effect of a bi-layered system on the retention of NaCl (for clarity only the Na^+ retention is shown). The selective membrane layers have identical material and adsorption properties, except for their different IEP, which are chosen arbitrarily. For the top layer IEP = 5.0 and for the second separating layer IEP = 8.3, as for γ-alumina. The achieved separation is compared to two monolayer membrane systems (having only one IEP), one with IEP = 5.0 and one with IEP = 8.3, respectively. The thickness of the separating layer in the monolayer systems is identical to the total thickness of the selective layers in the bipolar membrane.

The retention behaviour of the membranes with only one IEP in Fig. 3 is already explained in detail in many papers in the open literature. The general trend is a high retention far away from the IEP and zero retention at the IEP (the retention of a few percent at the IEP in Fig. 3 is caused by size exclusion).

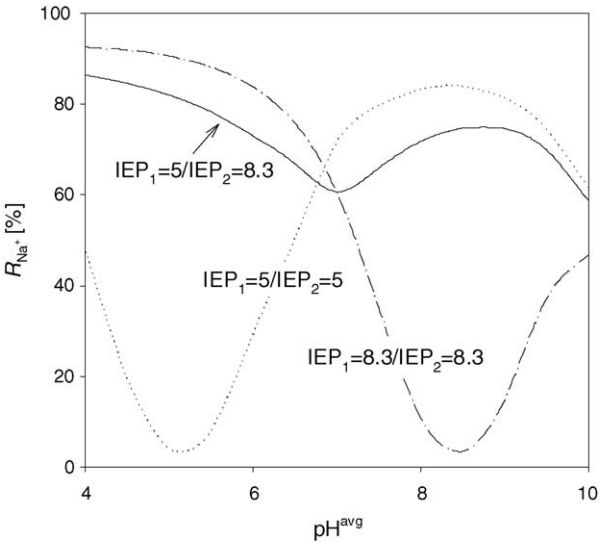

Fig. 3. Predicted Na^+ retention for NF membranes with two different or a single iso-electric point as function of pH for a solution of 1 mol/m^3 NaCl solution at 1 MPa. The iso-electric points of the top (1) and intermediate (2) layer are 5.0 and 8.3, respectively. The top and intermediate layers are γ-alumina (data from Table 2). Adsorption data for γ-alumina (except for the IEP) is used in the model calculations (see Table 1).

As expected, for the bi-layered membrane the separation performance is relatively constant: the retention of the two-layer system over the whole pH range varies between 60 and 80%. At the IEPs of the respective layers, $R \approx 80\%$, and this is a significant improvement compared to the performance of a monolayer membrane. There is, however, a small trade-off, because in the bi-layered system both layers contribute to retention, the overall retention is lower than that of a single material at a pH far removed from the IEP (e.g., at pH 4, $R \approx 90\%$ for the monolayer material with IEP = 8.3 while $R \approx 80\%$ for the bi-layered system).

3. Experimental

3.1. Membrane materials

Ceramic membranes, consisting of a silica and γ-alumina layer on top of an α-alumina support were prepared using sol–gel techniques. The α-alumina supports were prepared by filtering stabilised suspensions of AKP15 powder (Sumitomo Chemicals Ltd.) and consecutive sintering at 1150 °C. One layer of boehmite sol was applied on the support by dip-coating, resulting, after sintering at 600 °C, in the γ-alumina top layer. A more detailed description of the synthesis route for γ-alumina membranes has been reported elsewhere [20–23]. For the preparation of the silica membrane top layer a method reported by McCool et al. [24] was used. They describe the synthesis of a three-dimensional meso-porous cubic silica (MCM-48) membrane using a templating technique.

3.2. Determination of membrane charging behaviour

To access the charging properties of the membrane, electrophoretic mobility and potentiometric titration measurements were conducted. For these experiments the separating membrane layers were made as unsupported films, following the same preparation method as for the supported layers. Those films were then ground and suspended in 1, 10 and 100 mol/m^3 electrolyte solutions of NaCl at various pH. A detailed description of the preparation procedure of the solutions for the electrophoresis experiments is given elsewhere [9]. The potentiometric titration experiments were performed at the Physical Chemistry and Colloid Science Group of the University of Wageningen. A more detailed description of the techniques used for the determination of the membrane charging behaviour is given in Appendix A.

3.3. Water permeation

Assuming cylindrical pores, the (hydrodynamic) pore sizes of the separating layers can be determined by measuring the ultra-pure water flux. For γ-alumina this method has already been used previously and a pore size of 2.0 nm was obtained [9]. An explanation of this procedure is described in Appendix A.

3.4. Retention experiments

The ion retention experiments were performed at 25 ± 1 °C on a dead-end permeation set-up with a volume of 2 dm^3 under rapid stirring [9]. The retention experiments were conducted with aqueous solutions of 1 mol/m^3 NaCl at various pH. The pH was adjusted using 0.25 mol/m^3 NaOH and HCl.

During each pH experiment permeate samples were collected at a pressure difference of 1.8 MPa. The ion concentrations in the feed and permeate were determined with an ion-chromatograph (Dionex DX120). A period of 1 h was used to allow both the flux and the permeate retention to reach steady state. During this equilibration period, the permeate conductivity and flux were continuously monitored to assure that a steady-state situation had been reached.

4. Results and discussion

4.1. Membrane materials

In Fig. 4 a SEM micrograph of the ceramic membranes used for this study is shown. Contrary to the reports of McCool et al. [24], we did not obtain a meso-porous structure for the silica top layer. Instead, water permeation measurements showed that our silica had an average pore size in the micro-porous domain, slightly larger than that of non-templated silica. Also, XRD results (not shown) did not show any 3D cubic structure. Therefore, although the precise micro structure of the membrane top layer is unknown, in the remainder of this paper it will be referred to as micro-porous silica.

The thickness of the layers for the membrane used in this study was 1.9 mm for the support, 1.3 μm for the γ-alumina [25] and 0.4 μm for the silica. The thickness of the silica layer was obtained from SEM data.

Table 1
Adsorption properties for NaCl on γ-alumina and silica

Adsorption parameters γ-alumina [16]	$\log(K^+) = 8.3$, $\log(K_{Na}) = \log(K_{Cl}) = -0.7$, $C_1 = 1.2$ [C/(V m)], $C_2 = 50$ [C/(V m)], $c_{tot}^{//} = 1.33 \times 10^{-5}$ [mol/m^2]
Adsorption parameters silica ($c_{tot}^{//}$ from [17])	$\log(K^+) = 2.0$, $\log(K_{Na}) = \log(K_{Cl}) = -4.0$, $C_1 = 0.88$ [C/(V m)], $C_2 = 48$ [C/(V m)], $c_{tot}^{//} = 1.33 \times 10^{-5}$ [mol/m^2]

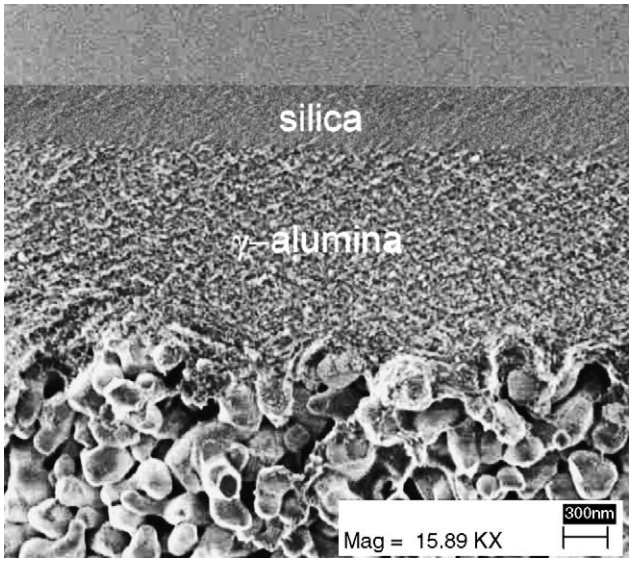

Fig. 4. SEM micrograph of silica/γ-alumina/α-alumina NF membrane.

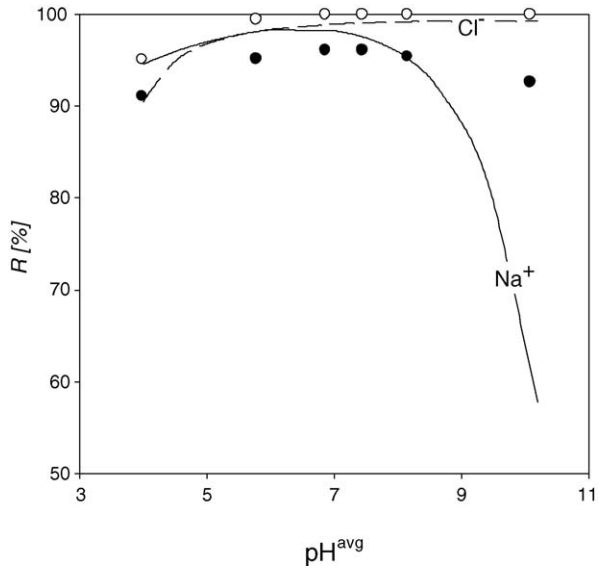

Fig. 5. Experimental silica/γ-alumina/α-alumina retention for Na^+ (black circles) and Cl^- (white circles) as a function of pH for 1 mol/m^3 NaCl at 1.8 MPa trans-membrane pressure. Lines are Na^+ (solid) and Cl^- (dashed) model predictions.

4.2. Comparison of measured and calculated retention

In this section, the experimentally determined retention of 1 mol/m^3 NaCl through a supported bi-layered silica/γ-alumina membrane as a function of pH is compared to the predictions obtained with our transport model [8]. The adsorption and material data used in the model calculations are given in Tables 1 and 2, respectively. This data was obtained using several experimental techniques. Their results and interpretation are explained in Appendix A.

The variation in the feed pH displayed in Table 2 was determined by measuring the pH at the beginning and the end of every retention experiment. The average of these two pH values was then used for the model calculations.

The results of the experimental and model retention are shown in Fig. 5. The measured retention of NaCl is high, between 90 and 100 ± 5%, over the whole pH range. The data for $4 < pH < 9$ indicate that the chloride retention is constantly about 5% higher than that of sodium.

The experimental results in Fig. 5 clearly indicate that separation performance of the bi-layered membrane is considerably better than for systems with only a γ-alumina layer. For γ-alumina membranes NaCl retentions of about 40% at pH ≈ 9.5 were reported (at 1.6 MPa, see [9]) while in the bi-layered system $R \approx 95\%$ in the alkaline region. This higher retention of the silica/γ-alumina system stems of course partly from the fact that the pore size of the silica layer is twice as small as that of the γ-alumina, but is also a direct result from the high (negative) membrane charge of the silica at neutral and alkaline pH. The high overall retention comes with a price however. The flux through the bi-layered system is about 10 times lower than that of a supported membrane with only a γ-alumina layer (see [9]).

The solid lines in Fig. 5 show the retention predictions using the transport model. For Na^+ at pH values between 4 and 9 and for Cl^- in the entire pH range the model retention predictions are in good agreement with the measurements (that is, within the experimental error in retention of 5%). For a pH of 4, however, the predicted chloride retention is lower than the sodium retention, in contrast with the experimental data.

Table 2
Measured solution and membrane properties

	pH^{avg}	Thickness (μm)	Permeability 10^{20} (m^2)	φ/τ	$2a$ (nm)
Silica	4.0 ± 0.5; 6.9 ± 0.1;	0.40	0.17	0.05	0.8 ± 0.2
γ-layer	7.4 ± 0.1; 5.8 ± 0.25;	1.3 (25)	2.3 [9]	0.17 [9]	2.0 ± 0.2 [9]
Support	10.1 ± 0.1; 8.2 ± 0.9[a]	1.9×10^3	15.8×10^3 [9]	0.09 [9]	197 ± 30 [9]

[a] Retention experiments performed in this order. Given pH deviations are variations between feed and retentate pH. In the table headings, φ and τ are the porosity and tortuosity of the respective layers and $2a$ denotes the average pore size.

At alkaline pH, both layers in the bi-layered system are negatively charged ($IEP_{silica} = 2.0$ and $IEP_{\gamma\text{-alumina}} = 8.3$) and therefore a lower sodium than chloride retention is expected because of the presence of highly mobile hydroxyl ions. The OH^- ions enhance the transport of sodium and hence reduce its retention. Both the experimental and the model results show this expected effect. However, the model predictions for sodium are a long way off from the measurements at pH 10. Where experimentally $R_{Na} = 93\%$ is found, the model predicts a retention of 58%. It is not clear what causes this large discrepancy but it is believed that its effect originates from structural changes in the silica [26] and concurrently it may also be that the parameters used to model the charging of silica (see Appendix A) are not valid anymore at such high pH values. The effect of structural changes will be discussed further in the following section on the membrane's pH stability.

In order to further understand the difference between the experimental data and the model predictions it is important to determine what the effect of both membrane separation layers is on the retention in different pH regions. To illustrate this, the contribution of the individual separating layers in the bi-layered system to the chloride retention as calculated with the model is shown in Fig. 6. It shows that for pH > 6 the membrane retention is completely determined by the silica layer. Therefore, the difference between the experimental and model retention in the alkaline pH region that we see in Fig. 5 points to an incomplete description of the silica layer by the model.

At pH < 6, Fig. 6 indicates that the γ-alumina layer starts to contribute significantly to the overall NaCl retention. At these acidic pH values, the model predicts a lower retention for chloride than for sodium (Fig. 5). The reason for this result is the increased contribution of the γ-alumina to the overall model membrane retention coupled to the increased concentration of highly mobile protons. The experimental results, however, show instead a higher chloride retention at acidic pH. As in a system with only a silica layer at low pH (negatively charged membrane) the chloride retention is higher than that of sodium (because of the direction of the axial electric field), the experimental results indicate that even at low pH the silica layer dominates the retention of the membrane.

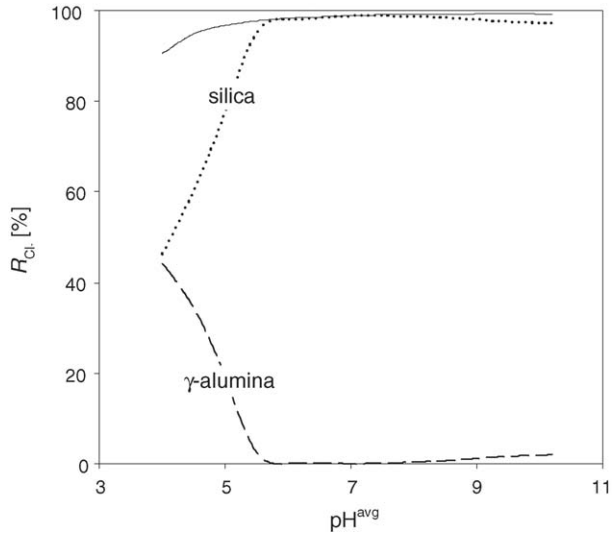

Fig. 6. Modeled contribution of the chloride retention for the silica (dotted line) and γ-alumina (dashed line) layers to the overall bi-layer model retention (solid line) for a silica/γ-alumina/α-alumina membrane as a function of pH for 1 mol/m^3 NaCl at 1.8 MPa trans-membrane pressure.

The analysis above shows that to describe the retention of a bi-layer NF membrane in a quantitative manner, it is important to accurately know the material (structure) properties of the individual layers. Because of the difficulty in determining the material parameters of the silica, the accurate prediction of the bi-layer retention over the entire pH region is hampered. Since an additional downside of the use of micro-porous silica material is its low trans-membrane flux, our aim for the future is to replace the silica top layer with a meso-porous titania layer, as titania can be much easier characterised and its meso-porous structure will result in a considerably higher flux.

4.3. Effect of solvent pore viscosity on retention

It is known that in confined geometries the viscosity of water μ^{pore} is higher than that in a bulk solution μ^{bulk} [27–31]. Andrade and Dodd [32,33] give an estimation of μ^{pore} as a function of the radial electric field E,

$$\mu^{pore} = \mu^{bulk}(fE^2 + 1). \quad (12)$$

For water, Lyklema [29] estimated the constant f to be 10.2×10^{-16} m^2/V^2. Eq. (12) indicates that as the radial electric field increases the pore viscosity decreases.

When Eq. (12) is used to calculate the viscosity in the silica pores of the bi-layered membrane it is found that the pore viscosity increases with increasing pH. This is simply because the silica pore potential (and thus the electric field) increases with increasing pH. The experimentally measured flux through the membrane during the retention experiments, however, shows an increased flux with increasing pH (Fig. 7), contrary to the trend predicted by Eq. (12). This experimental result therefore indicates that probably the viscosity in the membrane pores is not any different from its bulk value, and therefore throughout this study whenever convective transport had to be considered, the bulk viscosity (0.9 mPa s) was used.

4.4. Membrane pH stability

In previous work [9] it was already concluded that the stable pH range for γ-alumina was 4 < pH < 10. Therefore in this section the focus is only on the pH stability of the silica membrane top layer.

The observed effect in Fig. 7 of increasing flux with increasing pH could be due to a poor alkaline stability of the silica membrane. If this is the case, it could lead to dissolution of the top layer, resulting in an increase in the silica pore size and/or a reduction of the silica layer thickness. In literature it has been reported that some silicas prepared by templating techniques are stable for pH < 5.4 [26]. However, for another MCM-48 silica Nishiyama et al. [34] reported a stability up to pH 9. This ambivalence in the literature data seems to indicate that the pH

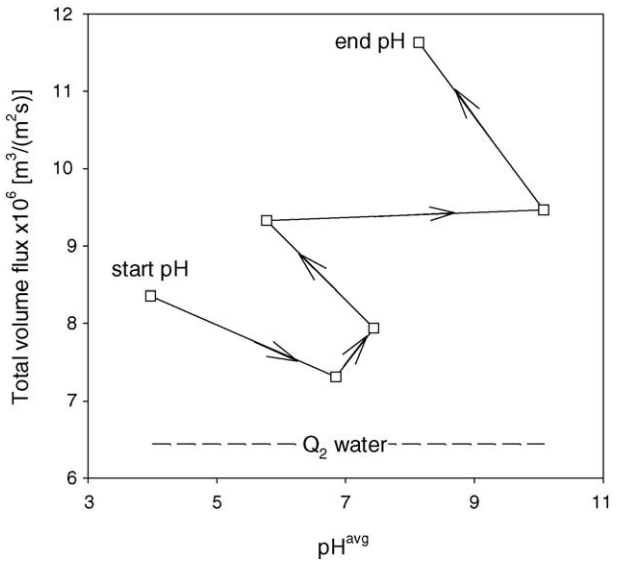

Fig. 7. Volume flux of 1 mol/m^3 NaCl through silica/γ-alumina/α-alumina membrane as function of pH^{avg} at 1.8 MPa trans-membrane pressure. Dashed line represents the initial flux of ultra-pure water at pH^{avg} = 5.8 and 1.8 MPa.

stability of templated silicas is dependent on their preparation history.

We believe that the specific templated silica used in this study was stable for 4 < pH < 10. This conclusion is based on the experimental results of the ultra pure water flux before and after the retention experiments, displayed in Fig. 8. Although Fig. 7 indicates that the flux through the silica layer is a strong function of pH, Fig. 8 shows that this pH effect is reversible as that the water flux after the retention experiments is the same (within experimental error) as the initial ultra pure water flux. Therefore, the effect of pH from the retention experiments on the structural properties (that is, the pore size and layer thickness) of the silica layer was negligible on the time scale of our measurements.

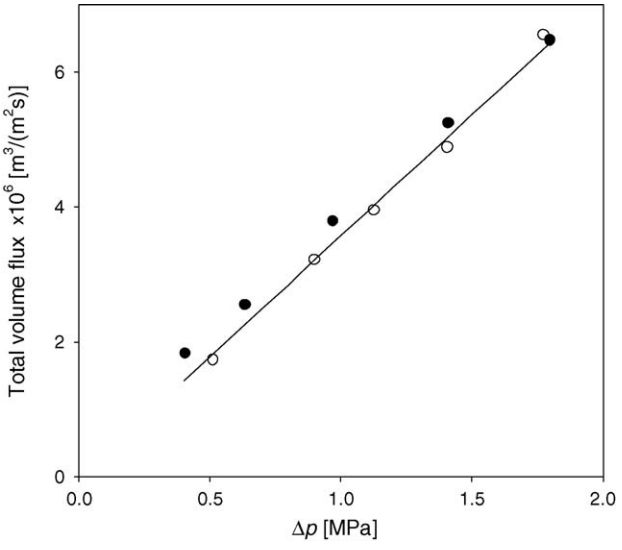

Fig. 8. Volume flux of ultra-pure water as a function of trans-membrane pressure before (white circles) and after (black circles) the complete series of retention experiments displayed in Fig. 5. Solid line is fit according to Eq. (A.1) of volume flux data collected before the series of retention experiments (white circles).

Apart from dissolution of the silica layer the change in flux with pH of Fig. 7 might also be due to a change in morphology of the templated silica material. Such structural changes were reported by Doyle and Hodnett [26]. They showed that MCM-48 changed its pore diameter in acidic conditions (pH < 5.4) by ≈20%. Using X-ray diffraction, they observed that the MCM-48 structure disappeared altogether at pH 6.9. Further transformations occurred at pH > 9.1. If the templated silica in our study exhibited such structural changes, they were apparently reversible (cf. Fig. 8) or had a minor influence on the transport properties in the silica layer of the membrane.

4.5. Influence of model input parameters on predicted overall retention

Apart from a physical origin, the discrepancy observed at alkaline pH between the experimentally measured sodium retention in Fig. 5 and the predicted model values can be due to errors in the input parameters used to describe the silica layer in the model. In order to establish whether this is the case a sensitivity analysis was performed on some of the key model input parameters for this layer, being its charging characteristics ($K_{Na\_Si} = K_{Cl\_Si}$, C_{1_Si}, C_{2_Si}), pore size ($2a_{Si}$) and permeability (B_0^{Si}). Their impact on the overall membrane retention predictions at pH 10.2 compared with the predictions shown in Fig. 5 are discussed below.

The adsorption parameters for silica were varied by ±50% of their base case value (e.g., log (K_{Na}) = −4.0 ± 2.0). This large variation, however, only resulted in a change of the overall NaCl retention of less than 1% at pH 10.2. Clearly, the retention is not very sensitive to the values of the adsorption constants in this pH region, which can be explained from the very high (zeta) potential on the silica layer. Fig. 10 shows that the zeta potential at pH 10.2 is around −80 mV (in the silica pores the uniform potential is −184 mV) and the exclusion from chloride from the membrane is therefore almost complete. Even a significant variation in the silica adsorption parameters cannot change this situation (cf. also [9] for the case of Ca^{2+} ions). The deviation between the observed and predicted retention at alkaline pH in Fig. 5 can therefore not be amended by changing the model's adsorption parameters.

Changing the flux through the bi-layered membrane by varying the permeability of the silica layer has a more significant impact on the predicted overall retention. Fig. 7 indicates that at high pH a 10–12 times higher flux is obtained. If B_0^{Si} is increased by a factor of 10, while keeping the pore size at 0.8 nm, the overall retention of chloride ions changes by <1%. The Na^+ retention, however, decreases by 15%. That is to be expected as the extra electrical field that is set up to prevent the transport of mobile charges in the membrane as a result of the increased flux favours the transport of co-ions through the system, thereby reducing the retention of sodium. To obtain a better agreement between the predicted and experimental retention we would therefore have to reduce the silica permeability, but this is in conflict with the experimental data in Fig. 7.

A change of the silica pore size, while keeping the permeability constant, will influence the membrane retention by means

of steric hindrance. A pore size variation of 50% was investigated. For $2a_{Si} = 1.2$ nm the change in the sodium and chloride retention change at pH 10.2 was within the numerical accuracy of the model (that is <2%). When $2a_{si}$ was decreased to 0.4 nm, however, R_{Na} decreased by 46% (R_{Cl} remained fairly unchanged). This can be understood by considering the competition between chloride and hydroxyl ion exclusion in the silica pore. For a smaller pore size the ratio of x_{Cl^-}/x_{OH^-} will increase as the much smaller hydroxyl ions can still more easily enter the pores. As OH^- is more mobile than Cl^-, the trans-layer axial potential gradient will be smaller, thereby decreasing the sodium retention.

If it would be assumed that the increase in permeability observed at alkaline pH (see Fig. 7) is solely due to an increase in the silica pore size, both B_0^{Si} and $2a_{Si}$ would have to be increased in the model. By setting $B_0^{Si} = 1.7 \times 10^{-20}$ and $2a_{Si} = 1.2$ nm (in keeping with the results in Fig. 7) the Na^+ retention at pH 10.2 increased by 9%, while R_{Cl} decreased by 4%. By making these adjustments in the model parameters, the model predictions are indeed in better agreement with the experimental data. However, the agreement is still poor and further improving it would mean that the model parameters would have to be set to physically unrealistic values.

5. Conclusions

The retention behaviour of supported bi-layered membranes for 1 mol/m^3 NaCl as a function of pH is determined experimentally and compared with the results of a predictive transport model. In general the model calculations agree well with the experimental data. At the extreme pH of 10 the sodium retention prediction is poor. The observed effect may be due to the uncertainty in the model's structure and charging parameters of the (templated) silica layer. To test if reducing this uncertainty in the model parameters will lead to a better agreement between the predicted and experimentally observed retention for a bi-layered membrane, in a future study the micro-porous silica layer will be replaced by a meso-porous titania that can be characterised much better and, additionally, will have a significantly higher flux.

Acknowledgements

The authors would like to thank Wika Wiratha and Alisia Peters of the Inorganic Material Science Group for the preparation of the membranes and Wim Threels of the Physical Chemistry and Colloid Science Group at Wageningen University for the potentiometric titration experiments.

Appendix A

A.1. Water permeation

In the water permeation experiments of the bi-layered membrane, the volume flow rate v is directly proportional to the trans-membrane pressure difference Δp,

$$v = B_0^* \Delta p. \tag{A.1}$$

If the thickness L and permeability of the support B_0^s and the γ-layer B_0^γ are known (see Table 2), the silica permeability B_0^{Si} can be calculated from the slope B_0^*, $1/B_0^* = \mu(L_s/B_0^s + L_\gamma/B_0^\gamma + L_{Si}/B_0^{Si})$. Fig. 7 shows the relation between the volume flux and pressure difference for the silica/γ-alumina/α-alumina membrane. Using this data the silica permeability was calculated to be 1.7×10^{-21} m^2.

Benes et al. [25] determined a porosity φ of 15–25% for silica using spectroscopic ellipsometry. In this work we have used the value $\varphi = 25\%$. Assuming a tortuosity τ of the silica layer of 3, equal to that of γ-alumina (see [9]), the pore size of the silica layer was determined to be 0.8 nm.

A.2. Determination of membrane charging behaviour

To extract the adsorption parameters (K^+, K_{Na}, K_{Cl}, C_1, C_2 and $c_{tot}^{//}$) from zeta potential data alone using the $1-pK$ triple layer (TL) model (see Section 2) may lead to ambiguous results because these parameters are strongly correlated [35]. Therefore we have combined information on the zeta potential with that of the surface charge and also experimental and literature data to fix some of the adsorption parameters in our work.

The surface charge σ_0 can be directly measured using potentiometric titration. In such an experiment, the templated silica is ground into particles, which are suspended in the desired electrolyte solution. The surface charge is then determined by the difference between the amounts of protons that produce a given pH in the silica suspension and the same pH in a blank sample (without silica) with only the electrolyte (here 1 mol/m^3 NaCl) present. For the determination of σ_0, 0.48 g of silica (specific surface area 492.65 m^2/g) was added to 53.5 ml of demineralised water. Next, small amounts of 500 mol/m^3 of HCl were added from a buret and the pH of the suspension was recorded. After each addition of acid the suspension was left until equilibrium had been reached (i.e. no change in the supension's pH was observed). The point of zero charge of silica is only reached at low pH. In this region the electrolyte solution is not thermodynamically ideal ($\gamma_i \neq 1$). Therefore, in the calculations of the surface charge the Davies relation (see Eq. (16) in [8]) was used to calculate the activity coefficients of the protons.

In Fig. 9, the surface charge of silica is given as a function of pH for 1 mol/m^3 NaCl. The data show a point of zero charge (PZC) at pH 2.0. The value of the PZC in this work is close to that of Bolt [36] and Tadros and Lyklema [37], who obtained pH_{PZC} 2.5–3.0. The surface charge should reach its PZC in an asymptotic manner (cf. the shape of the experimental data in [36,37]) and this is clearly not the case in our titration measurements. This is because the σ_0 data for pH < 3 in Fig. 9 have a high measurement uncertainty. One of the reasons for this high measurement error is the large amount of acid that has to be added to achieve a pH below 3. A small error in the determination of the amount of added H^+ will have a large impact on the calculated value of σ_0.

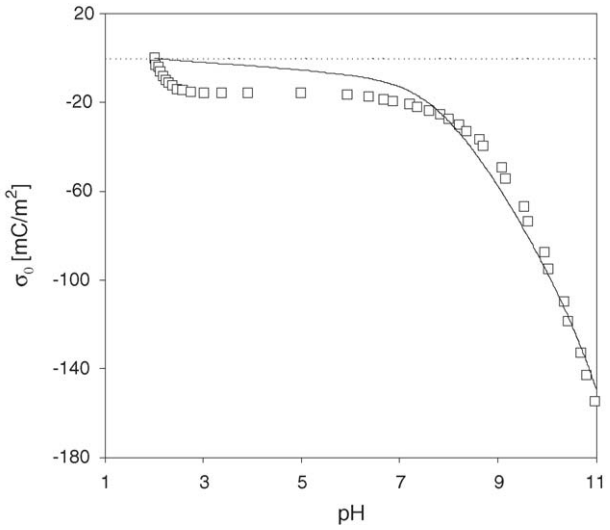

Fig. 9. Surface charge of silica as function of pH for a solution of 1 mol/m^3 NaCl solution. Solid line is the model calculation of the triple-layer model combined with a $1-\mathrm{p}K$ description of the surface adsorption chemistry.

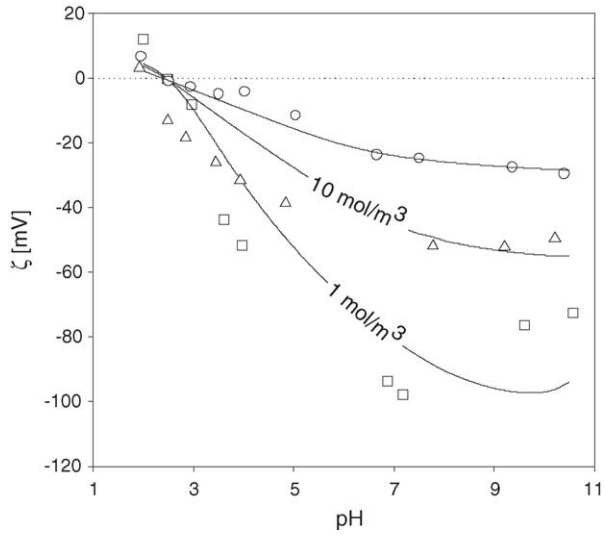

Fig. 10. Zeta-potential of silica as function of pH for NaCl solutions of 1 mol/m (squares), 10 mol/m^3 (triangles), and 100 mol/m^3 (circles). Solid lines are model calculations of the $1-\mathrm{p}K$ triple-layer model. The ζ-plane was located at $1\gamma_1$ (1 mol/m^3), $0.98\gamma_1$ (10 mol/m^3) and $0.96\gamma_1$ (100 mol/m^3) of the outer Helmholtz plane [16].

The solid line in Fig. 9 shows the $1-\mathrm{p}K$ TL model fit. A detailed description of the fitting of the adsorption parameters is given elsewhere [16]. Below we will briefly mention the important features for the fitting procedure. The total number of sites on the silica surface, $c_{\mathrm{tot}}^{//}$, was fixed at 8 sites/nm^2 using literature data [17]. Although there is some evidence suggesting that chloride adsorbs preferentially on silica [37] this effect, if present (see [36]), will be small. In this study NaCl is therefore assumed to act as an indifferent electrolyte. As a result of this, the adsorption constants for Na^+ and Cl^- were set equal in the fitting procedure ($K_{\mathrm{Na}} = K_{\mathrm{Cl}}$).

Because of the indifferent adsorption of NaCl it holds that $-\log(K^+) = \mathrm{pH_{PZC}} = \mathrm{pH_{IEP}}$ (with IEP and PZC the iso-electric point and point of zero charge of the material, respectively). Hence, during the fitting $\log(K^+)$ was kept fixed at 2.0 (see Table 2), in agreement with the experimental evidence for the surface charge and zeta potential (see next section). Hence, the three parameters that had to be determined were K_{Na}, K_{Cl} (with $K_{\mathrm{Na}} = K_{\mathrm{Cl}}$), and the Helmholtz capacities C_1 and C_2 (see Table 1). Two data sets were used for the determination of the adsorption parameters: the σ_0-pH and the ζ-pH data (see Fig. 10) at 1 mol/m^3 NaCl.

A.3. Zeta potential

The zeta potential of the silica material is obtained by electrophoresis [16]. The measured electrophoretic mobility of the silica membrane particles is converted into a zeta potential using the model proposed by O'Brien and White [38].

The measured zeta potentials and their fits with the $1-\mathrm{p}K$ TL model are displayed in Fig. 10 (the adsorption parameters were determined using only the ζ-pH data for 1 mol/m^3 NaCl). The experimental data show an iso-electric point at pH 2.0 ± 0.5. With increasing concentration the zeta potential is expected to decrease. For $\mathrm{pH} > \mathrm{pH_{IEP}}$ our experiments show this behaviour but at $\mathrm{pH} \leq 2.5$, however, the zeta potentials at 10 mol/m^3 lie below that of 100 mol/m^3 It not clear what causes this deviation in ζ at 10 mol/m^3.

References

[1] M.S. Hall, D.R. Lloyd, V.M. Starov, Reverse Osmosis of Multicomponent Electrolyte Solutions. Part II. Experimental Verification, J. Membr. Sci. 128 (1997) 39.
[2] J. Randon, A. Larbot, C. Guizard, L. Cot, M. Lindheimer, S. Partyka, Interfacial properties of zirconium dioxide prepared by the Sol–Gel Process, Colloids Surfaces 52 (1991) 241.
[3] J. Randon, A. Larbot, L. Cot, M. Lindheimer, S. Partyka, Sulfate adsorption on zirconium dioxide, Langmuir 7 (1991) 2654.
[4] A.E. Childress, M. Elimelech, Effect of solution chemistry on the surface charge of polymeric reverse osmosis and nanofiltration membranes, J. Membr. Sci. 119 (1996) 253.
[5] W.B.S. De Lint, P.M. Biesheuvel, H. Verweij, Application of the charge regulation model to transport of ions through hydrophilic membranes: one-dimensional transport model for narrow pores (nanofiltration), J. Colloid Interface Sci. 251 (2002) 131.
[6] T. Van Gestel, C. Vandecasteele, A. Buekenhoudt, C. Dotremont, J. Luyten, R. Leysen, B. Van Der Bruggen, G. Maes, Salt retention in nanofiltration with multilayer ceramic TiO_2 membranes, J. Membr. Sci. 209 (2002) 379.
[7] C. Labbez, P. Fievet, A. Szymczyk, A. Vidone, A. Foissy, J. Pagetti, Analysis of the salt retention of a titania membrane using the 'DSPM' model: effect of pH, salt concentration and nature, J. Membr. Sci. 208 (2002) 315.
[8] W.B.S. De Lint, N.E. Benes, Predictive charge-regulation transport model for nanofiltration from the theory of irreversible processes, J. Membr. Sci. 243 (2004) 365.
[9] W.B.S. De Lint, N.E. Benes, Separation properties of γ-alumina nanofiltration membranes compared to charge regulation model predictions, J. Membr. Sci. 248 (2005) 149.
[10] Y. Elmarraki, M. Cretin, M. Persin, J. Sarrazin, A. Larbot, Elaboration and properties of TiO_2-$ZnAl_2O_4$ ultrafiltration membranes, Mater. Res. Bull. 36 (2001) 227.
[11] M. Urairi, T. Tsuru, S.-I. Nakao, S. Kimura, Bipolar reverse osmosis membranes for separating mono- and divalent ions, J. Membr. Sci. 70 (1992) 153.

[12] L. Krasemann, B. Tieke, Selective ion transport across self-assembled alternating multilayers of cationic and anionic polyelectrolytes, Langmuir 16 (2000) 287.
[13] A.A. Sonin, G. Grossman, Ion transport through layered ion exchange membranes, J. Phys. Chem. 76 (1972) 3996.
[14] Y. Elmarraki, M. Persin, J. Sarrazin, M. Cretin, A. Larbot, Filtration of electrolyte solutions with new TiO_2-$ZnAl_2O_4$ ultrafiltration membranes in relation with the electric surface properties, Sep. Purif. Technol. 25 (2001) 493.
[15] T. Tsuru, S.-I. Nakao, S. Kimura, Ion separation by bipolar membranes in reverse osmosis, J. Membr. Sci. 108 (1995) 269.
[16] W.B.S. De Lint, N.E. Benes, A. Van Der Linde, J. Lyklema, M. Wessling, Determination of ion-adsorption parameters from zeta-potential measurements and titration data on a γ-alumina nanofiltration membrane, Langmuir 19 (2003) 5861.
[17] T. Hiemstra, J.C.M. De Wit, W.H. Van Riemsdijk, Multisite proton adsorption modeling at the solid/solution interface of (hydr)oxides: a new approach. II. Application to various important (hydr)oxides, J. Colloid Interface Sci. 133 (1989) 105.
[18] B.W. Ninham, V.A. Parsegian, Electrostatic potential between surfaces bearing ionizable groups in ionic equilibrium with physiologic saline solution, J. Theor. Biol. 31 (1971) 405.
[19] D.Y.C. Chan, J.W. Perram, L.R. White, T.W. Healy, Regulation of surface potential at amphoteric surfaces during particle-particle interaction, J. Chem. Soc. Faraday Trans. I 71 (1975) 1046.
[20] A.F.M. Leenaars, K. Keizer, A.J. Burggraaf, The preparation and characterization of alumina membranes with ultra-fine pores. Part 1. Micro structural investigations on non-supported membranes, J. Mater. Sci. 19 (1984) 1077.
[21] A.F.M. Leenaars, A.J. Burggraaf, The preparation and characterization of alumina membranes with ultrafine pores. 2. The formation of supported membranes, J. Colloid Interface Sci. 105 (1985) 27.
[22] A.F.M. Leenaars, A.J. Burggraaf, The preparation and characterization of alumina membranes with ultra-fine pores. Part 3. The permeability for pure liquids, J. Membr. Sci. 24 (1985) 245.
[23] R.J.R. Uhlhorn, M.H.B.J. Huis in't Veld, K. Keizer, A.J. Burggraaf, Synthesis of ceramic membranes. Part I. Synthesis of non-supported and supported γ-alumina membranes without defects, J. Mater. Sci. 27 (1992) 527.
[24] B.A. McCool, N. Hill, J. DiCarlo, W.J. DeSisto, Synthesis and characterization of mesoporous silica membranes via dip-coating and hydrothermal deposition techniques, J. Membr. Sci. 218 (2003) 55.
[25] N.E. Benes, G. Spijksma, H. Verweij, H. Wormeester, B. Poelsema, CO_2 sorption of a thin silica layer determined by spectroscopic ellipsometry, AIChE J. 47 (2001) 1212.
[26] A. Doyle, B.K. Hodnett, Stability of MCM-48 in aqueous solution as a function of pH, Micropor. Mesopor. Mater. 63 (2003) 53.
[27] D.C. Grahame, Effects of dielectric saturation upon the diffuse double layer and the free energy of hydration of ions, J. Chem. Phys. 18 (1950) 903.
[28] S. Basu, M.M. Sharma, An improved space-charge model for flow through charged microporous membranes, J. Membr. Sci. 124 (1997) 77.
[29] J. Lyklema, Fundamentals of interface and colloid science Solid-Liquid Interfaces, vol. II, Academic Press, London, 1995 (chapters 2 and 4).
[30] J.N. Israelachvili, Measurement of the viscosity of liquids in very thin layers, J. Colloid Interface Sci. 110 (1986) 263.
[31] M.L. Gee, P.M. McGuiggan, J.N. Israelachvili, A.M. Homola, Liquid to solid-like transitions of molecularly thin films under shear, J. Chem. Phys. 93 (1990) 1895.
[32] E.N.Da.C. Andrade, C. Dodd, Proc. R. Soc. (London) A187 (1946) 296.
[33] E.N.Da.C. Andrade, C. Dodd, Proc. R. Soc. (London) A204 (1951) 449.
[34] N. Nishiyama, H. Saputra, D.-H. Park, Y. Egashira, K. Ueyama, Zirconium-contain ing mesoporous silica Zr-MCM-48 for alkali resistant filtration membranes, J. Membr. Sci. 218 (2003) 165.
[35] R.E. Johnson Jr., A thermodynamic description of the double layer surrounding hydrous oxides, J. Colloid Interface Sci. 100 (1984) 540.
[36] G.H. Bolt, Determination of the charge density of silica sols, J. Phys. Chem. 61 (1957) 1166.
[37] Th.F. Tadros, J. Lyklema, Adsorption of potential-determining ions at the silica-aqueous electrolyte interface and the role of some cations, J. Electroanal. Chem. 17 (1968) 267.
[38] R.W. O'Brien, L.R. White, Electrophoretic mobility of a spherical colloidal particle, J. Chem. Soc. Faraday Trans. II 74 (1978) 1607.